Supplementary Information

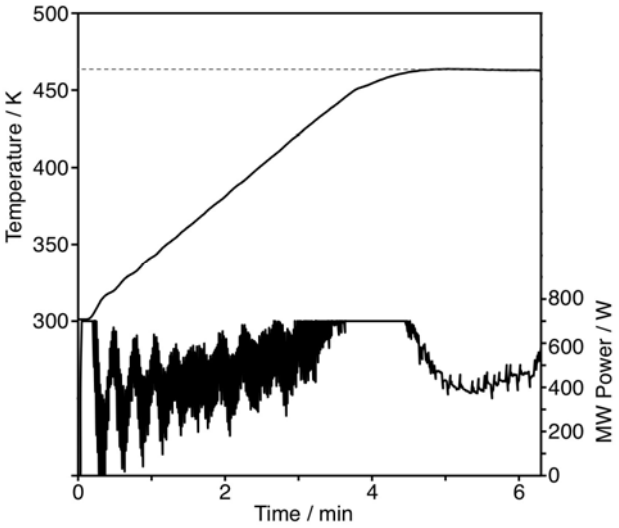

Figure S1. Time profile of both temperature and MW power during the synthesis of Cu_4Ni_6.

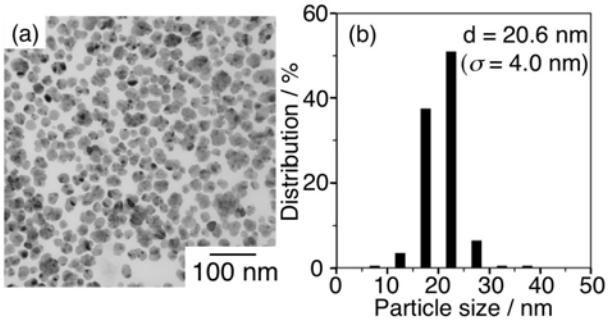

Figure S2. TEM image of Ni-2. The size distribution histogram was created using the diameters of 200 randomly selected particles shown in Figure S2-(a).

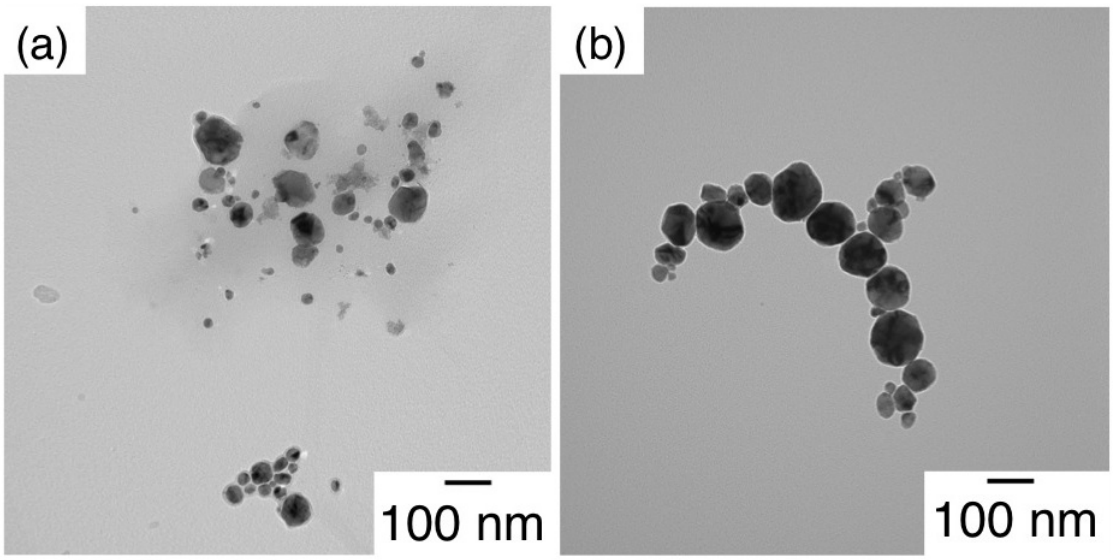

Figure S3. TEM images of Cu-1 (a) and Cu-2 (b).

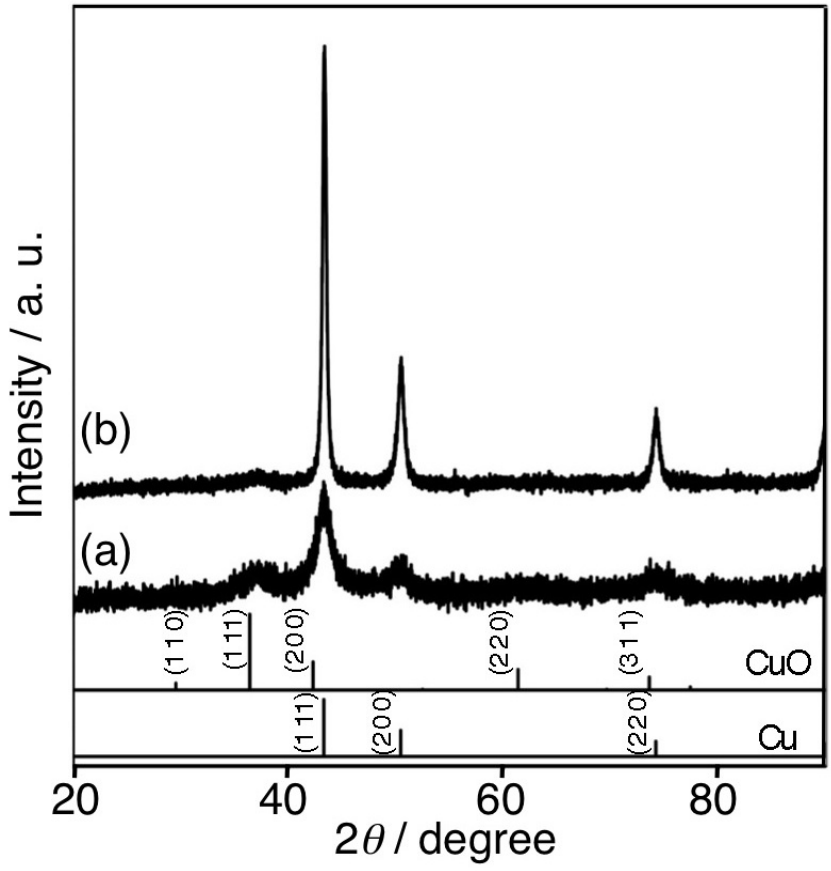

Figure S4. XRD patterns of Cu-1 (a) and Cu-2 (b).

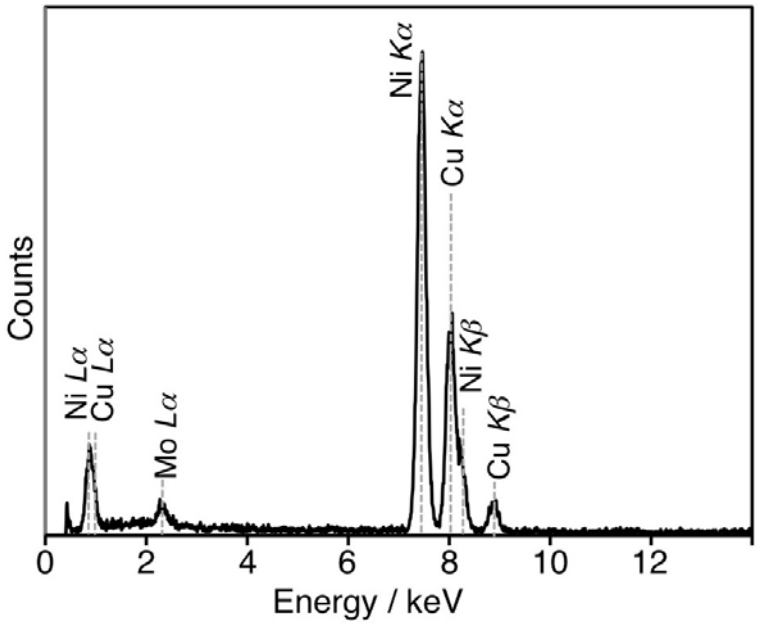

Figure S5. EDS spectrum of Cu_4Ni_6 nanoparticles. The sample was placed on a holey carbon film supported by a molybdenum grid. The Cu *K*α peak at around 8.0 keV overlapped with the Ni *K*β peak. The Cu *K*α intensities were calculated by waveform separation of the intensities of the peak at around 8.0 keV. Metal compositions of the Cu-Ni nanoparticle samples listed in Table 1 were calculated based on the Ni *K*α and Cu *K*α intensities calculated by waveform separation.

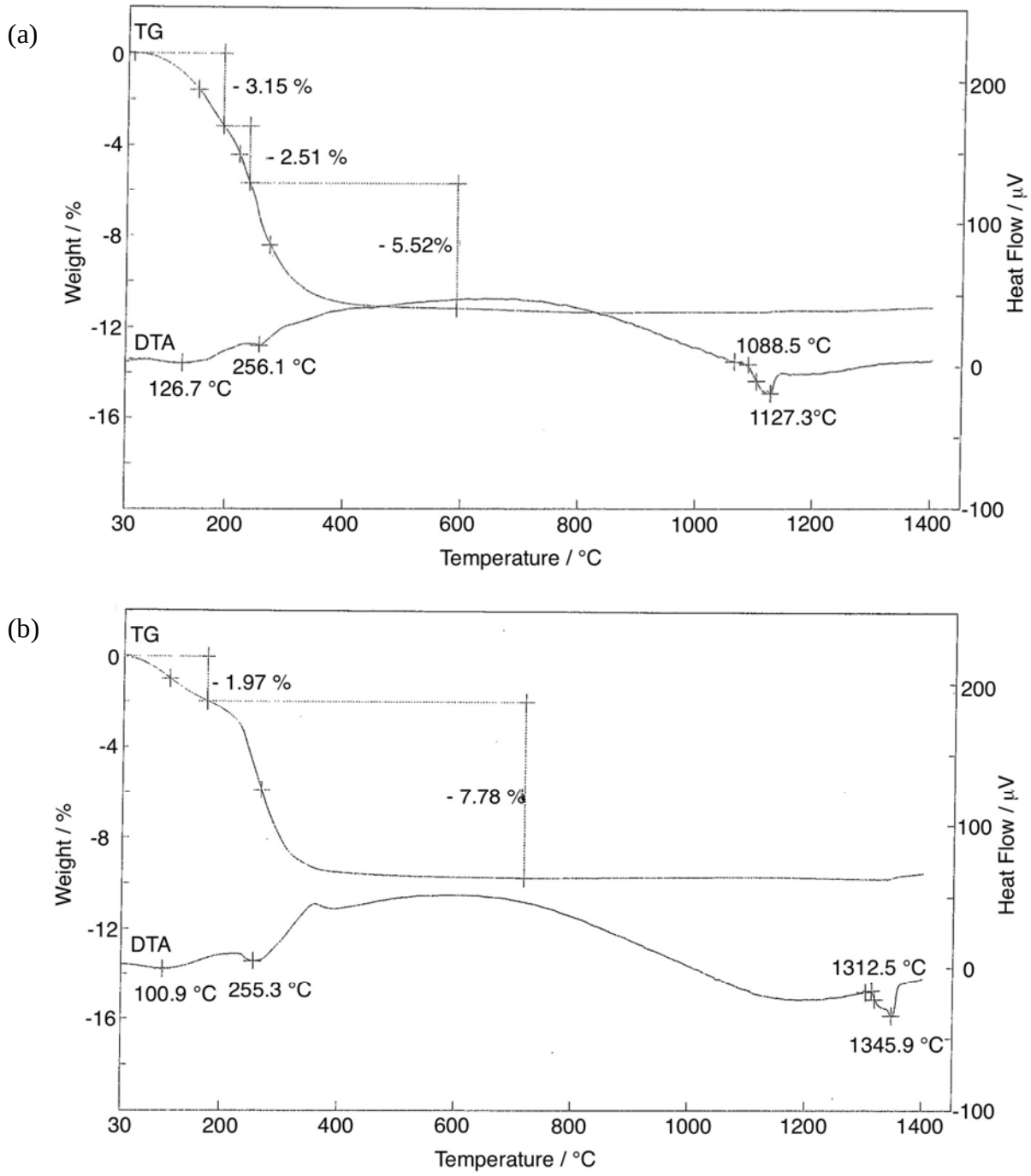

Figure S6. TG-DTA measurements of Cu_8Ni_2 (a) and Cu_3Ni_7 nanoparticles (b) at a heating rate of 20 °C min^{-1} under a nitrogen flow rate of 800 ml min^{-1}.

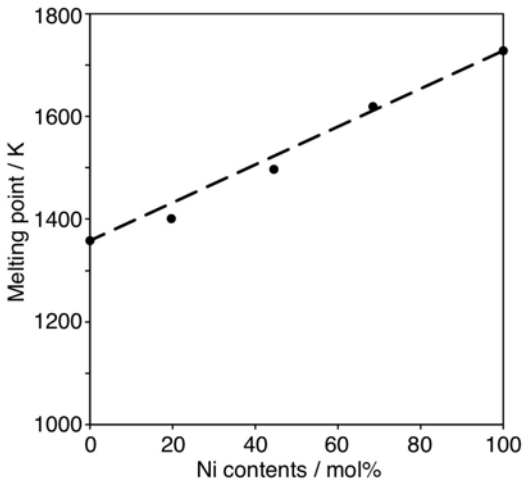

Figure S7. Melting points of Ni-1, Cu_3Ni_7, Cu_5Ni_5, Cu_8Ni_2 and Cu-2.

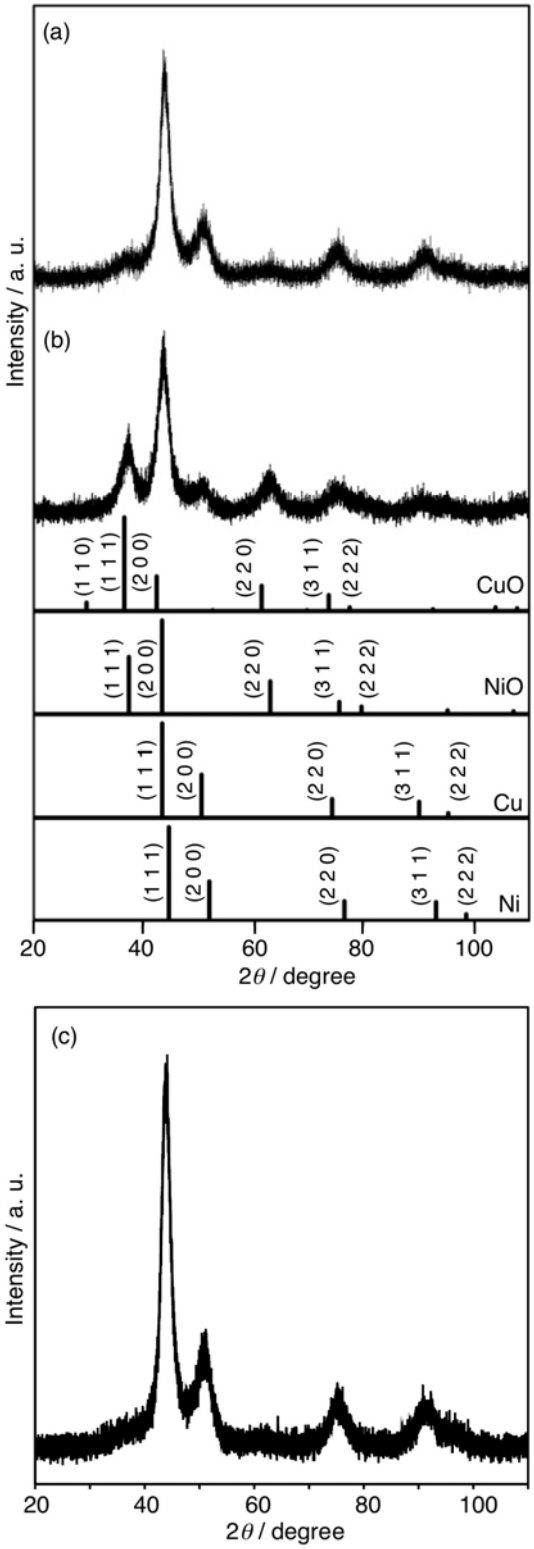

Figure S8. XRD patterns of Cu_4Ni_6 nanoparticle sample stored at 423 K (a) and 523 K (b) for 1h and stored for one year at room temperature (c) under air.

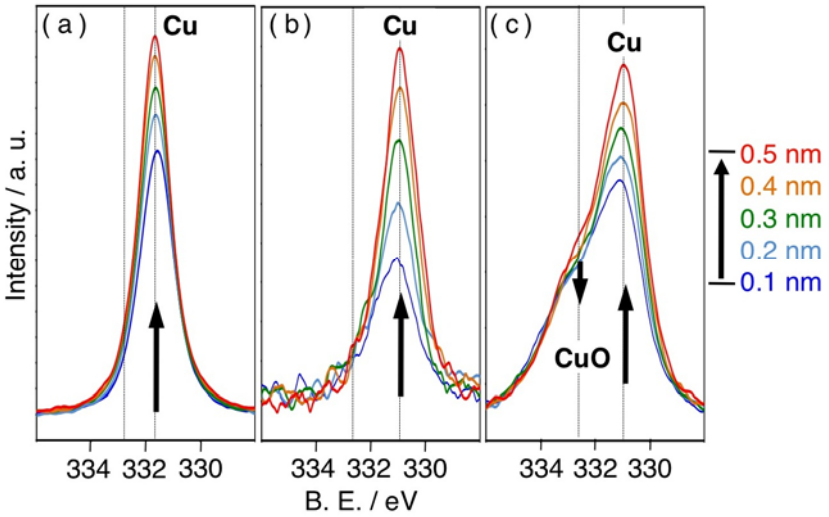

Figure S9. Cu $2p_{3/2}$ electron spectra of Cu-2 (a), Cu_4Ni_6 (b) and Cu_8Ni_2 (c).

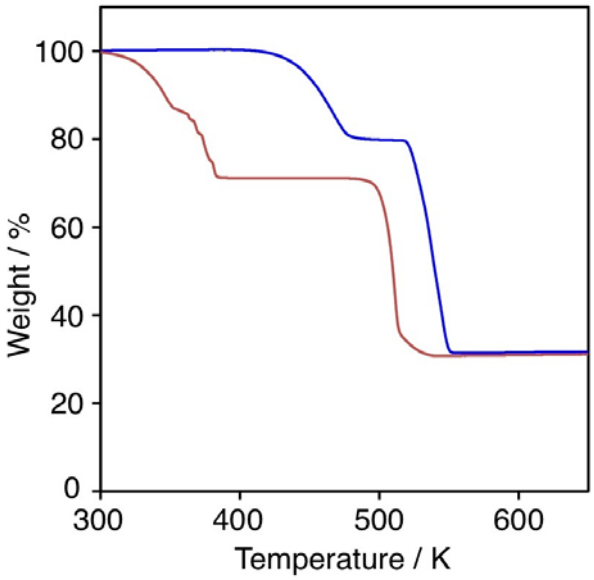

Figure S10. TG measurement of the neat formate salts at a heating rate of 10 K min^{-1} under a nitrogen flow rate of 100 ml min^{-1}, (a) nickel formate dihydrate (Blue line) and (b) copper formate tetra hydrate (Red line).

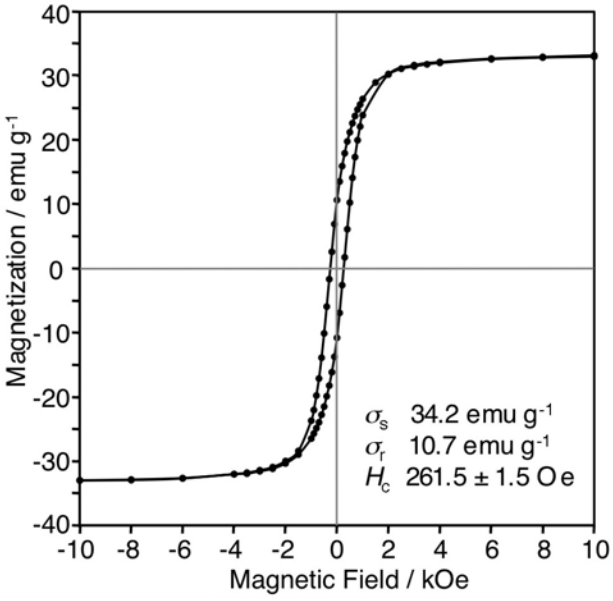

Figure S11. Magnetization versus applied field for Ni-2 in FC at 5 K.

Appendix 1.

The ratio of oleylamine molecules modified on the surface of Cu_4Ni_6 nanoparticles was estimated as follows. The Cu_4Ni_6 nanoparticles were oblate spheroid in shape with an eccentricity of 0.91 from TEM images (see Figures 2(a) and 2(b)). Major and minor axes were 11.7 nm and 4.9 nm, denoted as r_a and r_b, respectively. The eccentricity (e) was calculated from the formula ($e^2 = 1 - (r_b / r_a)^2$).

The volume ($V_{Cu\text{-}Ni}$), the surface area ($S_{Cu\text{-}Ni}$) and the weight ($W_{Cu\text{-}Ni}$) per one particle of these Cu-Ni nanoparticles was calculated according to the following formulas: (1), (2) and (3), respectively.

$$V_{Cu\text{-}Ni} = (\pi/3)\, r_a^2\, r_b \qquad : (1)$$

$$S_{Cu\text{-}Ni} = 2\pi\, [r_a^2 + (r_b^2 / 2e)\ln\{(1+e)/(1-e)\}] \qquad : (2)$$

$$W_{Cu\text{-}Ni} = 4\, V_{Cu\text{-}Ni}\, M_{Cu\text{-}Ni} / (a_{Cu\text{-}Ni}^3\, N_A) \qquad : (3)$$

(N_A ; Avogadro constant, $a_{Cu\text{-}Ni}$; lattice constant (3.580 Å), which was estimated from XRD analysis. The composition of Cu_4Ni_6 nanoparticles from TEM-EDS analysis was 39.3 atom%(Cu) and 60.7 atom%(Ni). The average molar weight ($M_{Cu\text{-}Ni}$) of Cu_4Ni_6 was calculated as described follows. $M_{Cu\text{-}Ni}$ = 0.393 x 63.55(Cu) + 0.607 x 58.69(Ni) = 60.60)

The content of long-chain amine (oleylamine) in the sample of Cu_4Ni_6 that was calculated based on weight loss, was ca. 10.0 wt%. The weight and the number of oleylamine ($W_{oleylamine}$ and $N_{oleylamine}$) modified on the surface of a particle was described as formulas (4) and (5), respectively.

$$W_{oleylamine} = (0.100 / 0.900)\, W_{Cu\text{-}Ni} \qquad : (4)$$

$$N_{oleylamine} = N_A\, W_{oleylamine} / 267.50 \qquad : (5)$$

Therefore, from the results of $S_{Cu\text{-}Ni} / N_{oleylamine}$, the molecules of oleylamine were modified on the surface of one particle (Cu_4Ni_6) at intervals of 17.3 nm^2.